HIGH AND LOW FREQUENCY ALFVÉN MODES IN TOKAMAKS

TH2/3

S. BRIGUGLIO, L. CHEN†, J.Q. DONG‡, G. FOGACCIA,
R.A. SANTORO*, G. VLAD, F. ZONCA
Associazione EURATOM-ENEA sulla Fusione,
C.P. 65, 00044 Frascati, Rome, Italy
† Department of Physics and Astronomy, University of California,
Irvine, CA 92697-4575, U.S.A.
‡ Southwestern Institute of Physics, Chengdu, China
* Naval Research Laboratory, Washington, D.C. 20375, U.S.A.

We present an analysis of the typical features of shear Alfvén waves in tokamak plasmas in a frequency domain ranging from the "high" frequencies ($\omega \cong v_A/2qR_0$; v_A being the Alfvén speed and qR_0 the tokamak connection length) of the toroidal gap to the "low" frequencies, comparable with the thermal ion diamagnetic frequency, ω_{*pi} and/or the thermal ion transit frequency $\omega_{ti} = v_{ti}/qR_0$ (v_{ti} being the ion thermal speed).

1. IDEAL MHD TAE SPECTRUM IN ITER

In the recent years, the shear Alfvén wave spectrum in laboratory plasmas has been extensively analyzed due to the possible excitations of these waves by resonant interactions with energetic particles such as charged fusion products and ions accelerated by plasma heating or current-drive systems. In particular, great attention has been devoted to the plasma eigenmodes near – or close to - the frequency gap [1] in the shear Alfvén continuous spectrum, i.e., Toroidal Alfvén Eigenmodes [2] (TAE) and Kinetic TAE [3] (KTAE), respectively.

Although a numerical approach to TAE and KTAE linear stability in a realistic plasma equilibrium is necessary, there still remain some concerns about the actual solution of this problem. In fact, in a tokamak reactor of major radius R_0 and minor radius a, the most unstable Alfvén modes will be characterized by toroidal mode numbers n in the range $\mathrm{a}/\rho_{LE} \gtrsim n \gtrsim \epsilon \mathrm{a}/\rho_{LE} \gg 1$, with $\epsilon = \mathrm{a}/R_0$ and ρ_{LE} the energetic particle Larmor radius. The large mode number is what creates serious resolution problems for conventional numerical simulations of these instabilities. Thus, significant insights can still be obtained with studies based on analytical-theoretical methods. Previous analyses – using a *2D-WKB* code [4] – have studied this problem either for (s, α) [5] (s being the magnetic shear and $\alpha = -q^2 R_0 \beta'$) model equilibria or for more general (but still model) equilibria, including possible shaping of magnetic flux surfaces [6]. In the former case, the fairly simple model equilibrium allowed us to focus on the details of the energetic particle dynamics and, thus, on the destabilization mechanism due to wave particle interactions. In the latter case, instead, a more precise description of the wave spectra in realistic geometries was obtained at the price of neglecting the energetic particle drive and all wave-particle resonant interactions; i.e., the result consist of calculations of a marginally stable set of global eigenmodes.

These investigations have confirmed that, under certain plasma conditions, TAE's can be shifted downward in frequency and out of the toroidal frequency gap in the Alfvén continuum. As a consequence, there is a great increase of mode damping due to finite coupling to the continuous spectrum. For high-n and the (s, α) model equilibrium [5], this has been shown to occur for $\alpha > \alpha_c(s)$ [7, 8, 9], i.e., above a critical threshold in the thermal plasma pressure gradient. In the present work, we further extend the approach of Ref. [6] and investigate the

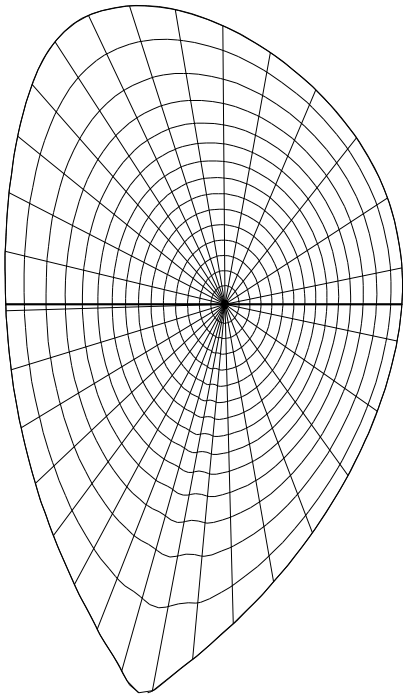

FIG. 1. Constant ψ and constant poloidal angle contours for the considered ITER equilibrium, indicated as ITER reference scenario #2 for TAE stability studies.

ideal MHD spectrum of high-n TAE modes in ITER, in order to explore the possibility of having plasma equilibria free of TAE modes. The ideal MHD assumption clearly prevents us from the computation of excitation thresholds, but allows us to analyze the conditions for enhanced TAE continuum damping in a *realistic* and completely general ITER equilibrium with shaped flux surfaces.

The plasma equilibrium we consider here is shown in Fig. 1 and is characterized by $R_0 =$ 8.14 m, $a = 2.90$ m, magnetic axis position $(R, Z) = (8.44$ m, 0.66 m), elongation $\kappa = 1.73$, $B_0 = 5.68$ T, plasma current $I = 20.9$ MA, volume average $< \beta >= 0.027$, poloidal $\beta_p = 0.69$, $q(0) = 0.84$ and $q(a) = 4.47$. Meanwhile, Fig. 2 shows the corresponding boundaries of the toroidal gap in the shear Alfvén continuous spectrum (i.e., the geometric *loci* of its accumulation points in the high-n limit). Here, and in the following of this section, frequencies are normalized to the Alfvén frequency on axis $\omega_A \equiv B_0/R_0\sqrt{4\pi\rho_0}$.

The frequency spectrum of TAE modes is found by solving the global dispersion relation [9]

$$\oint \theta_k\,(r;\omega)\,d\,(nq(r)) \;=\; (2p+w) \quad , \tag{1}$$

where $\theta_k \equiv k_r/nq'$ is the WKB eikonal entering in the expression of the radial *envelope* of the mode [9], p is the radial mode number and w is an integer defined in the following. The WKB eikonal θ_k is a function of the radial position, as it may be obtained from the solution of the local TAE dispersion relation

$$F\,(r,\theta_k;\omega) \;=\; 0 \quad , \tag{2}$$

which is parameterized by the mode frequency ω. Furthermore, the integration in Eq. (1) is extended to a complete periodic orbit (at fixed ω) in the (r,θ_k) phase-space, and w is either $w = 0$ for phase-space rotations or $w = 1$ for phase-space oscillations. Incidentally, we note that, in the up-down asymmetric equilibrium of Fig. 1, $\theta_k = 0$ and $\theta_k = \pi$ are not WKB turning points – as in the general symmetric case – and that turning point positions need to be determined numerically from Eq. (2).

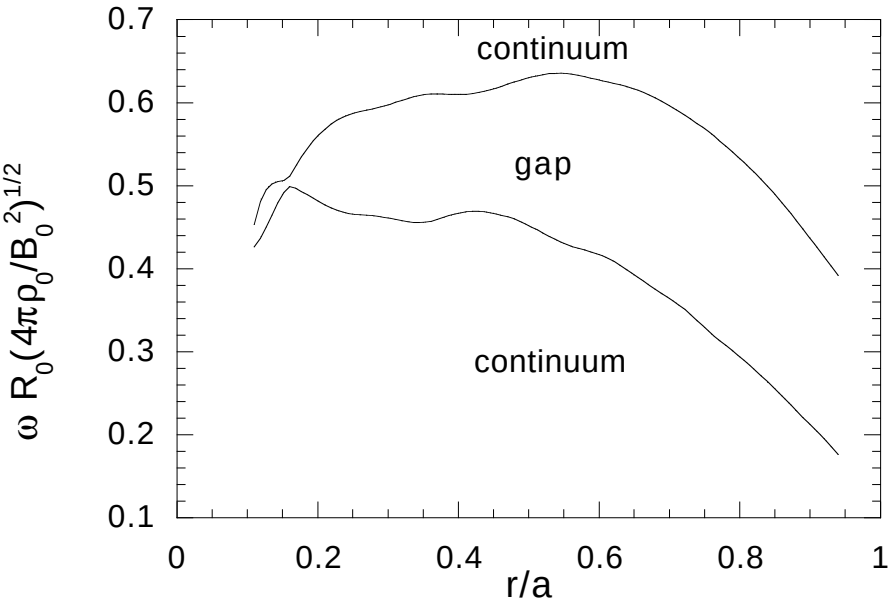

FIG. 2. Radial profile of boundaries of the toroidal Alfvén gap in the continuous spectrum.

Numerical solutions of the global mode dispersion relation are shown in Fig. 3 for the toroidal mode number $n = 20$. Each global mode is represented by an horizontal segment delimited by the WKB turning point positions, which give an estimate of the corresponding radial mode width. Different eigenmodes are labeled by the radial mode number p.

2. ENERGETIC PARTICLE MODES DYNAMICS

Besides the existence of eigenmodes of the thermal plasma, like TAE and KTAE, it has been shown that other instabilities may be *spontaneously excited* by a sufficiently strong energetic particle drive [10, 11]. These Energetic Particle Modes [10] (EPM), due to the non-perturbative contribution of particle dynamics in determining mode structures and frequencies, have linear and nonlinear behaviors which are different from those of TAE and KTAE. In particular, it has been demonstrated that, when the particle drive is large enough to exceed the EPM threshold, a strong redistribution in the energetic particle source can take place, yielding potentially large particle losses and, eventually, mode saturation [6]. Previous results from numerical simulations [6, 12] indicated that the EPM excitation threshold can be fairly high at low toroidal mode numbers n, although the tendency of the threshold to decrease for increasing n was also emphasized, in accordance with theoretical expectations [13], which predicted a minimum in the excitation threshold for $n \gtrsim \epsilon a/\rho_{LE}$.

Recalling that the linear excitation threshold of EPM corresponds also to the level above which a strong redistribution in the energetic particle source can take place, it becomes a crucial issue to investigate whether, for higher mode numbers n, the EPM excitation threshold can become comparable with the values which are relevant for an ignited plasma. In the present section, we present new results on this problem with the help of self-consistent numerical simulations (moderate-n; $n \leq 16$) using a gridless finite-size-particle modified version [14] of the original three-dimensional PIC hybrid MHD-gyrokinetic code [12].

Figure 4 shows the typical dependence of the EPM growth rate (normalized to ω_A) on the energetic particle β_E on axis, β_{E0}, for different n's. Here, fixed parameters are $\epsilon = 0.1$,

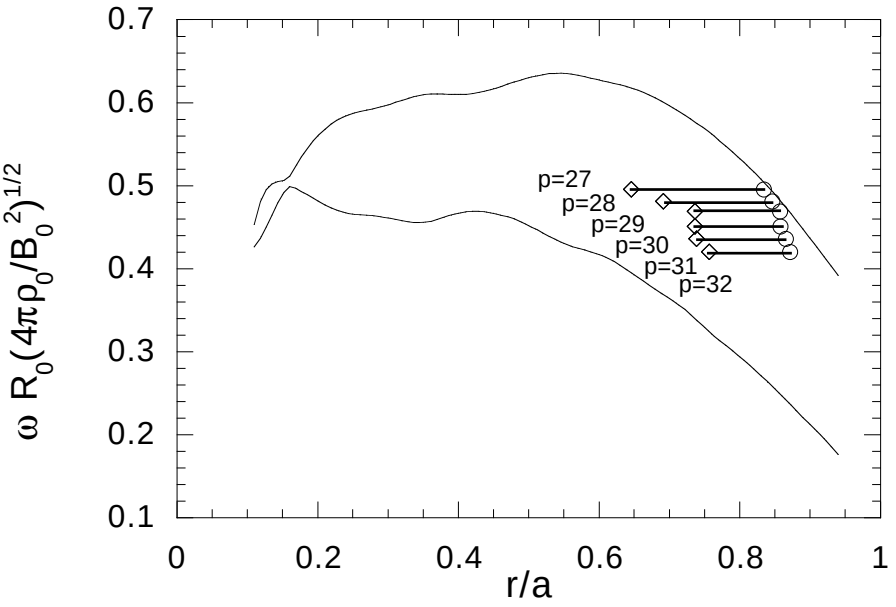

FIG. 3. Ideal MHD global TAE mode frequency spectrum for $n = 20$. The toroidal gap boundaries are also shown.

$q(0) = 1.1$, $q(\mathrm{a}) = 1.9$, $\rho_{LE}/\mathrm{a} = 0.01$ and $L_{pE}/R_0 = \epsilon(\mathrm{a}/r)^3/16$, with $L_{pE}^{-1} \equiv |\nabla p_E|/p_E$. The existence of an excitation threshold, β_{E0}^{th}, is apparent, above which the EPM growth rate rapidly increases with β_{E0}.

The dependence of β_{E0}^{th} on the toroidal mode number n is shown in Fig. 5 and it clearly indicates that a minimum of $\beta_{E0}^{th} \cong 7.5 \times 10^{-3}$ in the excitation threshold is reached for $n \cong 8$, for the present simulation parameters.

3. EXCITATION OF ALFVÉNIC ITG MODES

When the EPM frequency – because of either thermal plasma or energetic particle compression effects [6, 11, 15] – becomes so low to be comparable with the ion diamagnetic frequency ω_{*pi} and/or the thermal ion transit frequency $\omega_{ti} \equiv v_{ti}/qR_0$, the Energetic Particle Mode acquires all the characteristics of the so called Beta Induced Alfvén Eigenmode [16] (BAE) and it may be considered as a good candidate to explain some experimental observations [17]. Actually, it has been demonstrated that, for $\omega_{*pi} \approx \omega_{ti}$, BAE/EPM modes cannot be considered separately from modes of the Kinetic Ballooning Mode [18] branch resonantly excited by energetic particles, since they are two (generally coupled) branches of the shear Alfvén wave in this frequency range [19].

The BAE/EPM and KBM/EPM dispersion relation generally reads

$$i\Lambda\left(\frac{\omega}{\omega_{ti}}\right) = \delta W_f + \delta W_E \ , \tag{3}$$

where δW_f is the ideal MHD potential energy and δW_E is the contribution of energetic particles [19, 20]. Here, $\Lambda(\omega/\omega_{ti})$ is the *renormalized* plasma inertia in the presence of finite ω_{*pi} and ω_{ti}; i.e. [19]

$$\Lambda(x) = \beta_i^{1/2}\left\{x^2\left(1-\frac{\omega_{*pi}}{\omega}\right) + q^2 x\left[\left(1-\frac{\omega_{*ni}}{\omega}\right)F(x) - \frac{\omega_{*Ti}}{\omega}G(x) - \frac{N^2(x)}{D(x)}\right]\right\}^{1/2} \ , \tag{4}$$

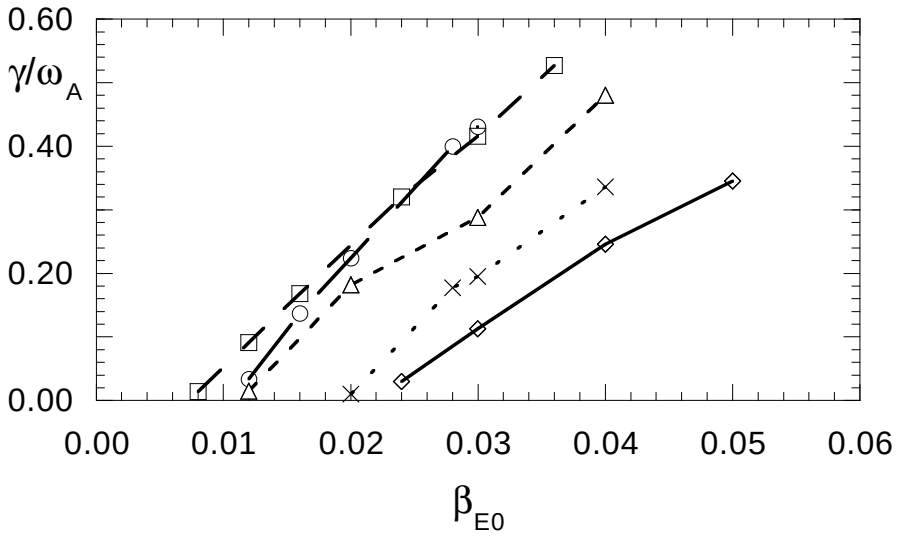

FIG. 4. Normalized EPM growth rates vs. β_{E0}, for different toroidal mode numbers; $n = 1(\diamond)$, $n = 4(\circ)$, $n = 8(\square)$, $n = 12(\triangle)$ and $n = 16(\times)$.

with

$$
\begin{aligned}
F(x) &= x(x^2+3/2)+(x^4+x^2+1/2)Z(x)\ , \\
G(x) &= x(x^4+x^2+2)+(x^6+x^4/2+x^2+3/4)Z(x)\ , \\
N(x) &= \left(1-\frac{\omega_{*ni}}{\omega}\right)[x+(1/2+x^2)Z(x)]-\frac{\omega_{*Ti}}{\omega}[x(1/2+x^2)+(1/4+x^4)Z(x)]\ , \\
D(x) &= \left(\frac{1}{x}\right)\left(1+\frac{T_e}{T_i}\right)+\left(1-\frac{\omega_{*ni}}{\omega}\right)Z(x)-\frac{\omega_{*Ti}}{\omega}[x+(x^2-1/2)Z(x)]\ , \qquad (5)
\end{aligned}
$$

$Z(x)=\pi^{-1/2}\int_{-\infty}^{\infty}e^{-y^2}/(y-x)dy$ being the plasma dispersion function. In Eq. (3), the excitation condition for EPM's of either the BAE or the KBM branch is $\mathbb{R}\mathrm{e}\delta W_E \leq \delta W_f$.

Another interesting feature of Eq. (3) is that it predicts that modes of the shear Alfvén branch may be excited even in the absence of an energetic particle drive. In fact, for $\delta W_E = 0$, it may be shown that the shear Alfvén continuous spectrum can have an *unstable* accumulation point ($\delta W_f = 0$) in the presence of a sufficiently strong thermal ion temperature gradient [19, 21, 22]. This fact, which stretches Eq. (3) beyond its applicability limit, is the clear indication that a discrete Alfvénic mode must exist below the marginal stability threshold for ideal MHD modes [19, 23]. In fact, the existence of a solution of $\Lambda(\omega/\omega_{ti}) = 0$ with $\mathbb{I}\mathrm{m}\omega > 0$, demonstrates that, at the ideal MHD marginal stability boundary ($\delta W_f = 0$), there still exists a free energy source to be tapped by instabilities, provided that ∇T_i is sufficiently strong.

Since, at $\delta W_f = 0$, the mode structure tends to become highly localized in the radial direction (*singular* within ideal MHD), finite ion Larmor radius (FLR) and finite drift-orbit width (FOW) effects become crucial to demonstrate that unstable discrete modes can actually exist for $\delta W_f > 0$. In fact, it is possible to show that these instabilities may be interpreted as a discretization of the *unstable continuum* due to FLR and FOW effects [23]. Since they are characterized by a shear Alfvén polarization and require ∇T_i to exceed a threshold value, they may be called shear Alfvén ∇T_i eigenmodes [23] (AITG), in analogy to their electrostatic counterpart. Using the (s, α) [5] model equilibrium for tokamak plasmas with shifted circular magnetic flux surfaces, we studied the problem of AITG excitation for $\delta W_f > 0$, using a set of integral eigenmode equations (quasi-neutrality and vorticity), which allow us to handle arbitrary $k_\perp \rho_i$ (FLR) and $k_\perp \rho_d$ (FOW).

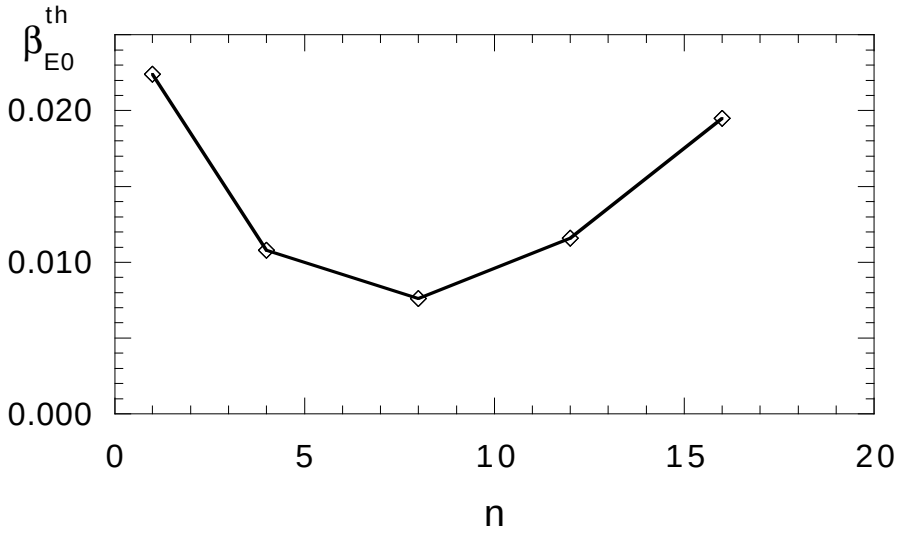

FIG. 5. Dependence of the EPM excitation threshold β_{E0}^{th} on the toroidal mode number n.

Numerical solutions of the coupled integral equations for the two fields $\left(\delta\phi, \delta A_{||}\right)$ indicate that the growth rate of AITG is maximum for $k_\theta \rho_{Li} \approx 0.3$ [24], with k_θ the poloidal wave vector and ρ_{Li} the thermal ion Larmor radius. Figures 6 and 7 show [24], respectively, the real and imaginary parts of the AITG mode frequency, normalized to ω_{*pi}, vs. α for three different values of $\eta_i = 0.5, 1.0, 2.5$. Fixed parameters are $s = 1$, $q = 1.5$, $k_\theta \rho_{Li} = 0.3$, $T_e/T_i = 1$, $\eta_e/\eta_i = 1$ and $L_{pi}/R_0 = 0.057$, with $L_{pi}^{-1} \equiv |\nabla p_i|/p_i$. For reference, also the "electrostatic" ITG is shown for $\eta_i = 2.5$.

It is apparent that the AITG instability can exist well below $\alpha_{crit} \cong 0.62$ the stability threshold for ideal ballooning modes [5] and that it is actually stronger than the usual electrostatic ITG for $0.4 \div 0.5 \lesssim \alpha/\alpha_{crit} \lesssim 1$. This fact can be explained with the stabilizing influence of magnetic field line bending. In fact, approaching MHD marginal stability, line bending stabilization is nearly balanced by the ballooning destabilization and the AITG mode is unstable because of the free energy available at the unstable continuum accumulation point. For $\alpha < \alpha_{crit}$, i.e. $\delta W_f > 0$, line bending stabilization becomes more and more effective, and the AITG mode is eventually completely stabilized.

Line bending, as it is well known, can also explain the finite-β stabilization of the e.s. ITG mode. In fact, for increasing α (β), the coupling to the e.m. shear Alfvén branch also increases while, at the same time, the stabilizing influence of line bending diminishes (since the ideal marginal stability is approached). As a consequence, the stabilizing influence on the e.s. ITG branch is expected to be strongest somewhere in between $\alpha = 0$ and $\alpha = \alpha_{crit}$, as it appears to be the case from Fig. 7. It could be argued that this should also be the point around which the most unstable mode should become that with an e.m. shear Alfvén polarization, although the e.s. ITG cannot be generally expected to be completely stabilized.

As a concluding remark, it is worth to emphasize that low frequency ($\omega \approx \omega_{*pi} \approx \omega_{ti}$) shear Alfvén instabilities may have significant implications to both energetic and thermal particle transports. In the former case, as EPM's of either the BAE or the KBM branch, they may be candidates to explain the experimental observation [17] of large energetic ion losses due to Alfvén waves with frequencies lower than that of TAE's. In the latter case, the AITG modes described in this section can be expected to affect, particularly, electron transports, since they are characterized by magnetic fluctuations and, contrary to electrostatic ITG, are not stabilized by finite-β effects.

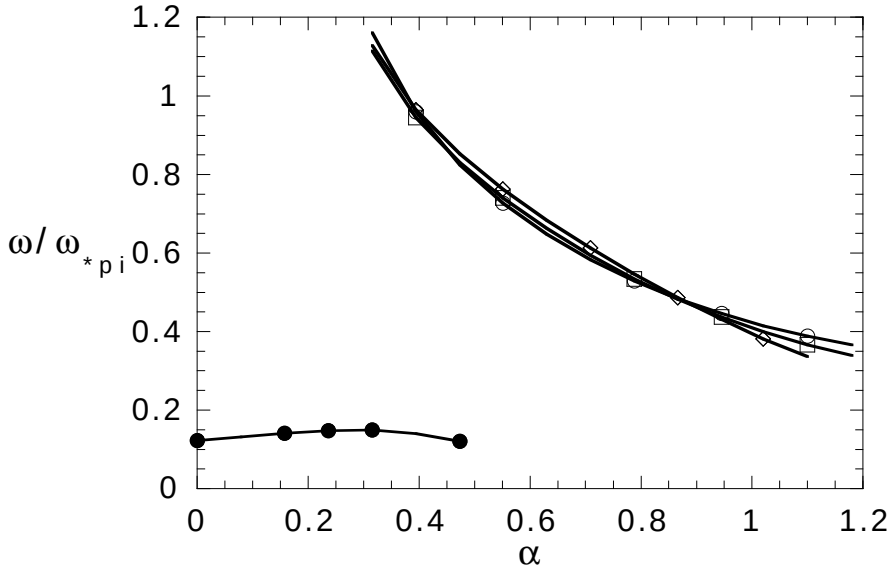

FIG. 6. Real mode frequencies of the AITG are shown vs. α for three different values of $\eta_i = 0.5(\circ), 1.0(\square), 2.5(\diamond)$. Fixed parameters are $s = 1$, $q = 1.5$, $k_\theta \rho_{Li} = 0.3$, $T_e/T_i = 1$, $\eta_e/\eta_i = 1$ and $L_{pi}/R_0 = 0.057$. The e.s. ITG ($\bullet$) is also shown for $\eta_i = 2.5$.

[1] KIERAS, C.E., and TATARONIS, J.A., J. Plasma Physics **28** (1982) 395.
[2] CHENG, C.Z., CHEN, L., and CHANCE, M.S., Ann. Phys. **161** (1985) 21.
[3] METT, R.R., and MAHAJAN, S.M., Phys. Fluids B **4** (1992) 2885.
[4] VLAD, G., *et al.*, Nuc. Fusion **35** (1995), 1651.
[5] CONNOR, J.W., HASTIE, R.J., and TAYLOR, J.B., Phys. Rev. Lett. **40** (1978) 396.
[6] BRIGUGLIO, S., CHEN, L., ROMANELLI, F., SANTORO, R.A., VLAD, G., ZONCA, F. , in the Proceeding of the 1996 IAEA Conference, Montreal (CAN), **F1-CN-64/DP-5** (1996).
[7] CHEN, L., in *Theory of Fusion Plasmas*, edited by J. Vaclavik, F. Troyon, and E. Sindoni, (Editrice Compositori, Bologna), (1989) 327.
[8] FU, G.Y., and CHENG, C.Z., Phys. Fluids B **2** (1990) 985.
[9] ZONCA F., and CHEN, L., Phys. Fluids B **5** (1993) 3668.
[10] CHEN, L., Phys. Plasmas **1** (1994) 1519.
[11] CHENG, C.Z., GORELENKOV, N.N., and HSU, C.T., Nucl. Fusion **35** (1995) 1639.
[12] BRIGUGLIO, S., *et al.*, Phys. Plasmas **2** (1995) 3711.
[13] ZONCA, F., CHEN, L., Phys. Plasmas **3** (1996) 323.
[14] BRIGUGLIO, S., *et al.*, Phys. Plasmas **5** (1998) 3287.
[15] SANTORO, R.A., and CHEN L., Phys. Plasmas **3** (1996) 2349.
[16] TURNBULL, A.D., STRAIT, E.J., HEIDBRINK, W.W., CHU, M.S., GREENE, J.M., LAO, L.L., TAYLOR, T.S., and THOMPSON, S.J., Phys. Fluids B **5** (1993) 2546.
[17] HEIDBRINK, W.W., STRAIT, E.J., CHU, M.S., TURNBULL, A.D., Phys. Rev. Lett. **71** (1993) 855.
[18] BIGLARI, H., and CHEN, L., Phys. Rev. Lett. **67** (1991) 3681.
[19] ZONCA, F., CHEN, L., SANTORO R.A., Plasma Phys. Contr. Fus. **38** (1996) 2011.
[20] TSAI, S.T., and CHEN, L., Phys. Fluids B **5** (1993) 3284.
[21] MIKHAILOWSKII, A.B., Nucl. Fusion **13** (1973) 259.
[22] KOTSCHENREUTHER, M., Phys. Fluids **29** (1986) 2898.
[23] ZONCA, F., CHEN, L., DONG, J.Q., and SANTORO, R.A., Paper 3B01, Int. Sherwood. Fus. Theory Conf., (1998).
[24] DONG, J.Q., private communication (1997).

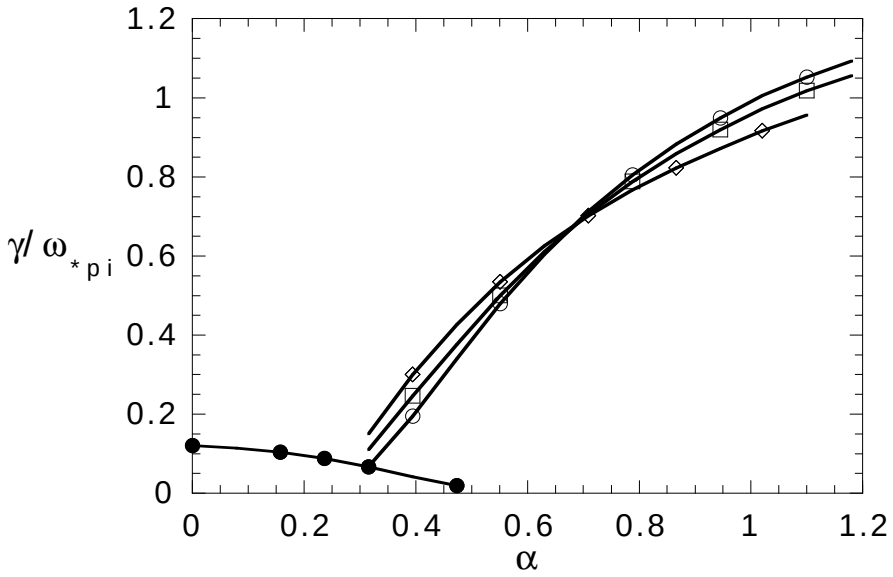

FIG. 7. AITG mode growth rates are shown vs. α for three different values of $\eta_i = 0.5(\circ), 1.0(\square), 2.5(\diamond)$ for the same parameters of Fig. 6. The e.s. ITG ($\bullet$) is also shown for $\eta_i = 2.5$.